Phosphatidylserine-Targeted Molecular Imaging of Tumor Vasculature by Magnetic Resonance Imaging

Heling Zhou PhD[1], Jason H. Stafford PhD[2], Rami Hallac PhD[1], Liang Zhang PhD[1], Gang Huang PhD[3], Ralph P. Mason PhD[1, 3], Jinming Gao PhD[2, 3], Philip Thorpe PhD[2], and Dawen Zhao MD,PhD[1, *]

[1] *Departments of Radiology, UT Southwestern Medical Center, Dallas, TX 75390, USA*
[2] *Departments of Pharmacology, UT Southwestern Medical Center, Dallas, TX 75390, USA*
[3] *Departments of Simmons Cancer Center, UT Southwestern Medical Center, Dallas, TX 75390, USA*

Phosphatidylserine (PS), normally restricted to the inner leaflet of the plasma membrane, becomes exposed on the outer surface of viable endothelial cells in tumor vasculature, but not in normal blood vessels. In the present study, we report the use of PGN635, a novel human monoclonal antibody that specifically targets PS, for *in vivo* molecular MRI of tumor vasculature. The F(ab′)$_2$ fragments of PGN635 were conjugated to polyethylene glycol (PEG) coated iron oxide nanoparticles (IO). Targeting specificity of the PS-targeted nanoprobes, IO-PGN635F(ab′)$_2$ was first confirmed by *in vitro* MRI and histological staining. *In vivo* longitudinal MRI was then performed before and after i.v. injection of IO-PGN635F(ab′)$_2$ into mice bearing breast 4T1 tumors. T_2-weighted MR images at 9.4 T revealed inhomogeneous signal loss in tumor as early as 2 h post injection. Furthermore, ionizing radiation induced a significant increase in PS exposure on tumor vascular endothelial cells, resulting in significantly enhanced and sustained tumor contrast ($p < 0.05$). Spatially heterogeneous MRI contrast correlated well with histological staining of tumor vascular endothelium. Our studies suggest that PS exposed within the lumen of tumor vasculature is a highly specific and useful biomarker for targeted MRI contrast agents.

KEYWORDS: *Phosphatidylserine (PS), Magnetic Resonance Imaging (MRI), Iron Oxide Nanoparticle, Tumor Vasculature, Breast Cancer, Radiation.*

INTRODUCTION

Molecular imaging of angiogenesis has recently been demonstrated using ligands that target biomarkers that are selectively expressed on tumor vasculature.[1–4] The integrin $\alpha_v\beta_3$, which is over expressed on the surface of tumor vascular endothelial cells, has been the most widely used target for imaging tumor angiogenesis. Various imaging contrast agents have been conjugated to $\alpha_v\beta_3$ binding ligands, such as Arginine-Glycine-Aspartic Acid (RGD)-containing peptide, for optical imaging, PET, SPECT and MRI.[3, 5–8] In addition to its over expression in angiogenic endothelial cells (EC), $\alpha_v\beta_3$ and several other integrins found to present abundantly on tumor cells play an important role on mediating interactions between tumor cells and their extracellular environment. A recent study by Schnell,

et al. has exploited [^{18}F] Galacto-RGD for PET imaging of $\alpha_v\beta_3$ expression in GBM patients.[9]

Phosphatidylserine (PS) is the most abundant anionic phospholipid of the cell membrane and is normally found on the inside of the cell. It is now known that PS becomes exposed on the outer surface of viable endothelial cells in tumor blood vessels.[10, 11] Studies have shown that characteristics of tumor environment, in particular, hypoxia, acidity, inflammatory cytokines and the elevated oxidative stress contribute to PS exposure on ECs.[10, 12] Vascular endothelium in normal tissues, even in those highly angiogenic ovarian blood vessels during ovulation, lacks exposed PS.[13] Along with its localization on vascular lumen, PS represents an ideal biomarker for vascular targeted imaging. Thorpe's lab has developed a series of monoclonal antibodies that recognize PS with higher specificity than does annexin V.[10, 14, 15] Several of these antibodies bind to PS complexed with the PS-binding protein, β2-glycoprotein I (β2GP1).[15, 16] Bavituximab, a chimeric monoclonal PS-targeting antibody, is in

advanced clinical trials in patients with lung and breast cancer.[17]

A new, fully human monoclonal PS targeting antibody, PGN635 has recently been developed.[18] Like bavituximab, PGN635 has a high specificity and affinity to PS ($K_d \approx 10^{-10}$ M). We have previously conjugated the F(ab′)$_2$ fragments of PGN635 to an NIR dye, IRDye800CW. The 800CW-PGN635F(ab′)$_2$ enabled sensitive and clear optical imaging of glioma mouse models.[18] However, due to its inherent low spatial resolution and penetration depth, optical imaging is not ideal to provide spatial information about intratumoral distribution of the probes. The goal of this study was to determine if PGN635F(ab′)$_2$ could be used to generate a MRI contrast agent that specifically targets tumor vasculature. MRI is a commonly used imaging modality with high spatial resolution and excellent soft tissue contrast. We conjugated amino-terminal PGN635F(ab′)$_2$ to carboxyl groups on the distal terminus of PEG chains that are coated on the surface of superparamagnetic iron oxide nanoparticles (SPIO). Specificity of IO-PGN635F(ab′)$_2$ binding to exposed PS was first studied *in vitro* on cultured vascular endothelial cells and tumor cells by histological staining and MRI. High field 9.4 T MRI was then applied to detect T_2-weighted signal intensity change in subcutaneous 4T1 tumors post i.v. injection of IO-PGN635F(ab′)$_2$. Radiotherapy is known to increase PS exposure on vascular endothelium. Therefore, to explore whether IO-PGN635F(ab′)$_2$ could be used to monitor dynamic changes in levels of exposed PS, 4T1 tumors were imaged after irradiation and differences in spatial distribution and quantity of IO-PGN635F(ab′)$_2$ was analyzed. Histological analysis of Prussian blue staining and immunohistochemistry were finally used to confirm that IO-PGN635F(ab′)$_2$ localized to the vasculature in tumor tissues.

METHODS

Preparation of PGN635F(ab′)$_2$ Fragments and Labeling with IO Nanoparticles

The human monoclonal antibody PGN635 was generated by Affitech A.S. (Oslo, Norway) in collaboration with Peregrine Pharmaceuticals. Inc., (Tustin, CA). It was produced under serum-free conditions by Avid Bioservices (Tustin, CA). Aurexis is a human monoclonal antibody that binds to an irrelevant antigen (*S. aureus* clumping factor A) and was used as a negative control antibody. PGN635 and Aurexis F(ab′)$_2$ fragments were generated by reacting antibodies with pepsin at a molar ratio of 1:130 (antibody:pepsin) for 1 hr at 37 °C. F(ab′)$_2$ fragments ($M_W = 110$ kD) were purified by FPLC using an S-200 column (Pharmacia, Piscataway, NJ) and PBS running buffer. F(ab′)$_2$ fragments were then conjugated to polyethylene glycol (PEG) coated super paramagnetic iron oxide (SPIO) nanoparticles with the iron oxide core diameter of 20 nm (SPP-20; Ocean Nanotech, AR). Briefly,

carboxyl (–COOH) group on the distant terminus of the PEG chain of SPIO (1 mg) were activated with 1-ethyl-3-[3-dimethylaminopropyl] carbodiimide hydrochloride (EDC) and *N*-hydroxysuccinimide (NHS) for 15 min, resulting in a semi-stable NHS or sulfo-NHS ester, which were reacted with amino-group-containing antibody fragments (1 mg) at room temperature for 2 hrs with continuous mixing to yield amide bond. The conjugates were separated from unbound antibody fragments overnight at 4 °C by using a DynaMag™ (Invitrogen, Grand Island, NY) magnetic separator. The products are referred to as IO-PGN635F(ab′)$_2$ or IO-AurexisF(ab′)$_2$. The iron concentration of IO-F(ab′)$_2$ was determined by atomic absorption spectrometer (SpectrAA 50 spectrometer; Varian Inc., Palo Alto, CA). The core size and hydrodynamic size of the nanoparticles before and after conjugation were measured by transmission electron microscope (JEOL-1200EX, Japan) and dynamic light scattering using Zetasizer Nano ZS (Malvern Instruments, Worcestershire, UK). MRI relaxivity was measured with various iron concentrations of the conjugates embedded homogeneously in 0.8% agarose. By fitting the values of $1/T_1$ or $1/T_2$ at different concentrations, the relaxivities r_1 and r_2 were determined.

The number of antibody fragments that were bound to each iron oxide nanoparticle was estimated by measuring the fluorescence intensity of near infrared dye labeled IO-F(ab′)$_2$. F(ab′)$_2$ was first labeled with IRDye-800CW (Li-COR, Lincoln, NE), as described previously.[18] The 800CW-F(ab′)$_2$ was then conjugated with iron nanoparticles using aforementioned procedures. Optical light intensity of 800CW-F(ab′)$_2$ or IO-F(ab′)$_2$-800CW at various concentrations was obtained at the emission wavelength of 778 nm and used to determine the number of F(ab′)$_2$ using a Maestro imaging system (CRI Inc. Woburn, MA).[19]

In Vitro Binding Specificity of IO-PGN635F(ab′)$_2$

Adult bovine aortic endothelial (ABAE) cells (Clonetics, Walkersville, MD) and 4T1 mouse breast carcinoma cells (American Type Cell Collection, Rockville, MD) were maintained in Dulbecco modified Eagle medium supplemented with 10% FBS and 2 mM L-glutamine. To induce PS exposure, the cells were treated with a single dose of 6 Gy X-radiation. 24 hrs later, the irradiated or sham irradiated cells were incubated with IO-PGN635F(ab′)$_2$ or the control IO-AurexisF(ab′)$_2$ at a concentration of 36 μg/ml iron for 1 hr. For the blocking study, the cells were pretreated with full length PGN635 (710 μg/ml) for 1 hr prior to IO-PGN635F(ab′)$_2$. Unbound particles were washed away with PBS, and then the cells were fixed with 4% paraformaldehyde (PFA). Prussian blue staining was performed to stain iron and counterstained by nuclear fast red.

In Vitro MRI of Binding Specificity of IO-PGN635F(ab′)$_2$

4T1 cells that were irradiated or sham irradiated 24 hrs earlier were incubated with IO-PGN635F(ab′)$_2$ at different concentrations (18, 36 and 61 μg/ml iron) or IO-AurexisF(ab′)$_2$ (36 μg/ml iron) for 1 hr. The same blocking study was performed here. After washing off all the unbound particles with PBS, 3×10^5 cells were mixed homogeneously with 0.8% agarose in 96-well-dish. The phantoms were imaged on a 9.4-T horizontal bore magnet with a Varian INOVA Unity system (Palo Alto, CA). A fast spin-echo multi-slice sequence (FSEMS; TR = 3000 ms, effective TE ranging from 40 to 120 ms with a 20 ms increment, average = 2, number of slices = 10, acquisition time = 10 min) was used to acquire T_2-weighted images and obtain quantitative T_2 values.

Tumor Model

All animal procedures were approved by the Institutional Animal Care and Use Committee of University of Texas Southwestern Medical Center. Two million 4T1 cells in 100 μl of serum-free medium containing 25% Matrigel (BD Biosciences, San Jose, CA) were injected subcutaneously on both thighs of anesthetized mice ($n = 12$; BALB/c nu/nu, 6–8 weeks old; NCI, Frederick, MD). Animals were sedated with 3% isoflurane and maintained under general anesthesia (2% isoflurane).

Radiation Treatment

When subcutaneous tumors on both thighs reached 6–8 mm in diameter, a single dose of 12 Gy of irradiation was delivered to the tumors on the left thigh using a small animal irradiator (XRAD320; Precision X-ray, Inc, North Branford, CT) fitted with a variable collimator to generate a single adjustable collimated iso-dose beam of X-rays at a dose rate of 10 Gy/min.

Detection and Quantification of Exposed PS *In Vivo*

Mice bearing two thigh tumors were given a single dose of 12 Gy irradiation to the left tumor to induce exposed PS, as described above. Twenty-four hours later, 150 μg of PGN635 or the control body Aurexis were injected i.v. and allowed to circulate for 4 hrs. The mice were anesthetized, exsanguinated, and perfused with heparinized saline. The tumors on both sides and adjacent muscular tissues were removed and frozen for preparation of cryosections. Vascular endothelium was stained using a rat anti-mouse CD31 antibody (BD Biosciences, San Jose, CA) followed by Cy3-labeled goat anti-rat IgG. PGN635 or Aurexis was detected using goat anti-human IgG conjugated to Cy2. Doubly labeled endothelial cells (i.e., CD31 positive/PGN635 positive) were identified by yellow fluorescence on merged images. The percentage of doubly positive vessels was calculated as follows: (mean number of yellow vessels per field/mean number of total vessels) $\times 100$. Ten random 0.079 mm^2 fields were evaluated for each section.

In Vivo MRI of Vascular Targeted IO-PGN635F(ab′)$_2$ Nanoprobes in 4T1 Tumors

When the subcutaneous tumors reached ~ 5 mm in diameter, *in vivo* MRI studies at 9.4 T magnet were conducted 24 hrs after radiation. Animals were sedated with 3% isoflurane and maintained under general anesthesia (1.5% isoflurane). Animal body temperature and respiration were monitored and maintained constant throughout the experiment (SA Instruments Inc., Stony Brook, NY, USA). The same FSEMS sequence as used for *in vitro* study was applied for *in vivo* image acquisition. A series of FSEMS (number of slices = 10) images was acquired before and at different time points, typically 2, 4, 8, 24 and 48 hrs after i.v. injection of IO-PGN635F(ab′)$_2$ ($n = 6$) or IO-AurexisF(ab′)$_2$ ($n = 4$; 2.5 mg iron/kg body weight in 120 μl volume) via a tail vein.

Analysis of MRI data was performed on a home written MATLAB program on both pixel-by-pixel and region of interest (ROI) basis.[20] ROIs were drawn on both the tumors and adjacent thigh muscles on the high resolution T_2-weighted images. Signal intensity (SI) in these ROIs was measured for all the echoes of FSEMS images and a ratio of tumor to muscle (TMR) was obtained. To provide the spatial distribution of IO-PGN635F(ab′)$_2$ nanoprobes in tumors, 'hot-spot' maps showing the area with significantly low SI was created based on a pixel by pixel analysis. Hot-spots were identified as voxels with SI values (based on effective TE = 80 ms) lower than 2 standard deviation of the baseline tumor parenchyma. Hot-spots were then overlaid on the corresponding high resolution T_2-weighted images. The total area of the hot-spots in individual MRI slices was summed and then divided by the whole tumor area to obtain the fraction of hot-spots.

Histological and Immunohistochemical Analysis

Immediately after MRI scanning, tumor-bearing mice were sacrificed and tumor tissues were harvested. The cryosections were immunostained with antibodies to the endothelial marker, CD31 (BD Biosciences) followed by horseradish peroxidase (HRP)-conjugated goat anti rat secondary antibody (Serotec, Raleigh, NC). The same sections were then used for Prussian blue staining to detect IO-PGN635F(ab′)$_2$ nanoprobes and observed under microscope to localize IO-PGN635F(ab′)$_2$ and their overlapping with tumor vascular endothelial cells.

Statistical Analysis

Statistical significance was assessed using an analysis of variance (ANOVA) on the basis of Fisher's protected least significant difference (PLSD; Statview; SAS Institute Inc., Cary, NC) or Student's t tests.

RESULTS
Characterization of IO-PGN635F(ab′)$_2$ Nanoprobes

The average hydrodynamic size of IO nanoparticles before conjugation was 23.3 nm compared to 24.1 nm on the manufacturer's manual (Fig. 1). After conjugation the average hydrodynamic size of IO-PGN635F(ab′)$_2$ became 24.7 nm (Fig. 1). IO-PGN635F(ab′)$_2$ had a Zeta potential as −5.8 mV. MRI relaxivity of IO-PGN635F(ab′)$_2$ at 9.4T was obtained: $r_1 = 0.064$ mM^{-1} s^{-1} and $r_2 = 255.3$ mM^{-1} s^{-1}, indicating it as a strong T_2 contrast agent. Based on the measurement of fluorescence intensity produced from NIR-800CW dye conjugated to IO-PGN635F(ab′)$_2$, we estimate that approximately 18 antibody fragments are attached to each nanoparticle via a covalent bond between the amino group of the antibody and the distal terminus of the polyethylene glycol (PEG) coated on the nanoparticle. No precipitation was visible in the solution of the conjugates for at least 2 weeks.

PS-Targeting Specificity of IO-PGN635F(ab′)$_2$ Nanoprobes *In Vitro*

Under the normal culture condition, there was essentially no PS exposure on cells. To induce exposure of PS on the outer membrane of the cells, adult bovine aortic endothelial (ABAE) cells and 4T1 breast cancer cells were irradiated 24 hr earlier with a single dose of 6 Gy to induce exposure of PS on the outer membrane of the cells. For both cell types, specific binding of IO-PGN635F(ab′)$_2$ to PS was observed exclusively on the irradiated cells (Figs. 2(B) and (E)), but not on the non-irradiated cells (Figs. 2(A) and (F)), evidenced by Prussian blue staining of irons (Figs. 2(B) and (E)). The blue staining appeared to be surrounding the cells, indicating the IO-PGN635F(ab′)$_2$ was bound on the cell surface. The control conjugate IO-AurexisF(ab′)$_2$ did not bind to the cells (Fig. 2(C)) The specificity of IO-PGN635F(ab′)$_2$ was further confirmed by pre-incubating with non-labeled PGN635 to block the binding of IO-PGN635F(ab′)$_2$ (Fig. 2(D)).

In Vitro MRI of PS-Targeting Specificity of IO-PGN635F(ab′)$_2$ Nanoprobes

T_2-weighted fast spin echo MRI was used to evaluate agarose phantoms containing 4T1 cells that were pre-incubated with various SPIO conjugates. In good agreement with the *in vitro* histological data, a marked reduction of SI was observed only in IO-PGN635F(ab′)$_2$-treated cells that were irradiated with 6 Gy (Fig. 3(A)).
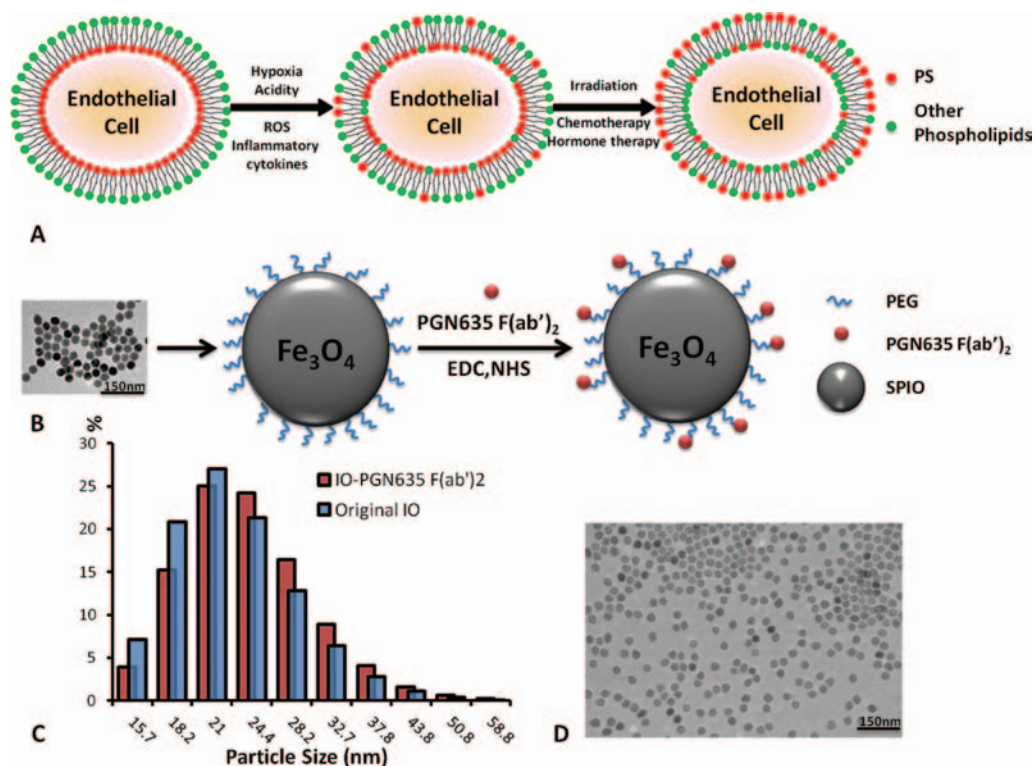
Figure 1. Phosphatidylserine (PS)-targeted MRI nanoprobe, IO-PGN635F(ab′)$_2$ (A) Schematic illustration of asymmetric distribution of PS (red dots) in tumor vascular endothelial cell membrane over normal vascular endothelial cells as a result of environmental stress in tumors. PS exposure can be further increased by therapy, such as ionizing irradiation or chemotherapeutic drugs. (B) Uniform sized IO nanoparticles coated with PEG have a core diameter of 20 nm and a hydrodynamic diameter 23 nm. IO was conjugated with the F(ab′)$_2$ of PGN635, a novel fully human monoclonal antibody that binds to PS. (C) and (D) Light scattering and TEM analysis were applied to evaluate particle size, showing uniform size distribution of IO-PGN635F(ab′)$_2$ with a mean hydrodynamic diameter of 25 nm.

4
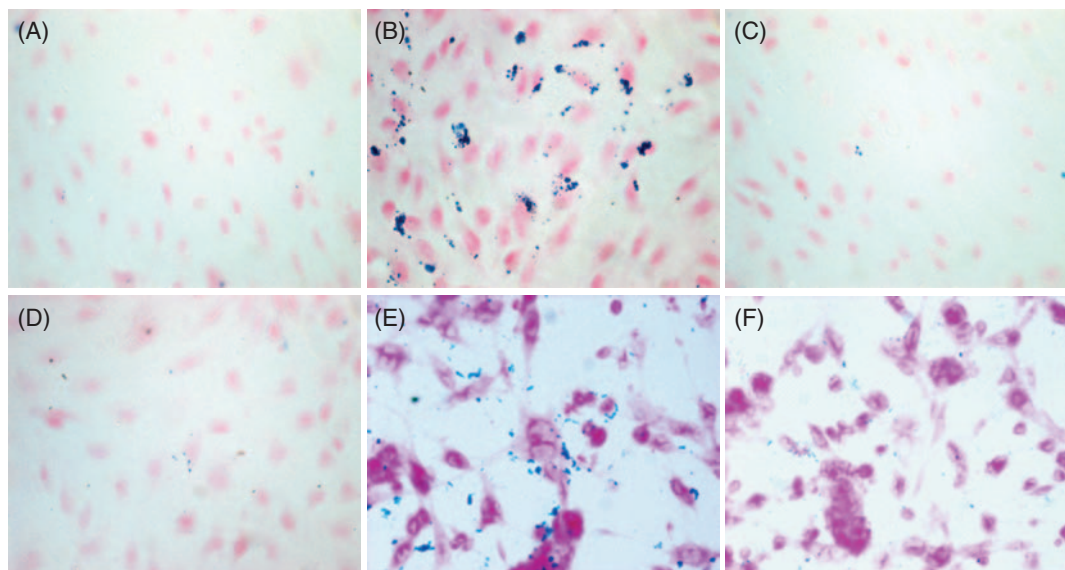
Figure 2. Prussian blue staining to evaluate the specificity of IO-PGN635F(ab′)$_2$ binding to exposed PS on the surface of vascular endothelial cells. *In vitro* ABAE endothelial cells were either untreated (A) or pre-treated with 6 Gy radiation (B)–(D) 24 hr earlier. The cells were then incubated with IO-PGN635F(ab′)$_2$ (A) and (B) or the control antibody conjugates, IO-AurexisF(ab′)$_2$ (C), and the binding was detected by Prussian blue staining (counterstaining with nuclear fast red). Abundant blue iron staining was observed on the irradiated cells (B), but not on the non-irradiated cells (A) or the irradiated cells incubated with IO-AurexisF(ab′)$_2$ (C). The specificity of IO-PGN635F(ab′)$_2$ was further confirmed by the competition study, showing significantly reduced binding after pre-treatment of the cells with PGN635 (D). Similarly, cell membrane localization of IO-PGN635F(ab′)$_2$ was detected on the irradiated 4T1 tumor cells (E), while a little blue staining was found on the non-irradiated 4T1 tumor cells (F).

A clear gradient of increased darkness was associated with increasing concentrations of the probes (Fig. 3(A)). Minimal change of the signal observed for cells incubated with IO-AurexisF(ab′)$_2$- or cells pre-incubated with non-labeled antibody. Again confirming the specific binding of IO-PGN635F(ab′)$_2$ to exposed PS. Quantitative measurements of spin–spin relaxation time (T_2) showed significantly shortened T_2 values in the irradiated cells treated with IO-PGN635F(ab′)$_2$, as compared to the control cells treated with PBS or the non-irradiated counterpart (Figs. 3(B) and (C); $p < 0.05$). A maximal reduction on T_2 was observed for the highest concentration of IO-PGN635F(ab′)$_2$ (Figs. 3(B) and (C)).

Exposed PS on Blood Vessels of 4T1 Tumors *In Vivo*

An average of $28 \pm 8\%$ of blood vessels in non-irradiated tumors had exposed PS on their endothelium, as judged by coincident staining of vessels by PGN635 and anti-CD31 (Fig. 4). Twenty-four hours after a single dose of 12 Gy, PGN635 binding was significantly increased indicating increased levels of exposed PS in the tumors. PGN635 staining predominantly co-localized with tumor vessels ($61 \pm 8\%$; $p < 0.001$; Fig. 4).

In Vivo MRI Detection of IO-PGN635F(ab′)$_2$ in 4T1 Tumors

Longitudinal MRI was performed before and after i.v. injection of IO-PGN635F(ab′)$_2$ or IO-AurexisF(ab′)$_2$.

As shown in Figure 5, increased intratumoral hypointense regions, caused by specific binding of IO-PGN635F(ab′)$_2$ to exposed PS, were clearly visualized in both the non-irradiated and irradiated tumors as early as 2 hrs post IO-PGN635F(ab′)$_2$, as compared to pre-injection baseline images. Inhomogeneous distribution of the nanoprobes appeared throughout the tumors. As expected, irradiation significantly enhanced PS exposure, resulting in more IO-PGN635F(ab′)$_2$ binding than that in the non-irradiated tumor. Follow-up MRI showed that the darkened regions in the irradiated tumor became more evident at 8 hr and persisted up to 48 hrs post injection. The time course of normalized tumor/muscle ratio (TMR) of T_2-weighted signal intensity showed a minimal TMR value at 2 hr for both the non-irradiated ($22 \pm 7\%$) and irradiated ($34 \pm 9\%$) tumor, which gradually recovered to the baseline level in the non-irradiated tumor, but stayed at low level in the irradiated tumor (Fig. 5(B)). Histological analysis confirmed that blue stained IO-PGN635F(ab′)$_2$ co-localized with CD31-positive endothelial cells in non-irradiated tumor tissues (Fig. 5(C)). Consistent with imaging data, there were more IO-PGN635F(ab′)$_2$ nanoprobes binding to blood vessels of the irradiated tumors (Fig. 5(D)).

Spatial 'Hot-Spots' Analysis of Intratumoral Distribution of IO-PGN635F(ab′)$_2$

To provide better understanding of the spatial distribution of IO-PGN635F(ab′)$_2$ in tumor, 'hot-spots' maps of the hypointense regions were created. Post IO-PGN635F(ab′)$_2$,
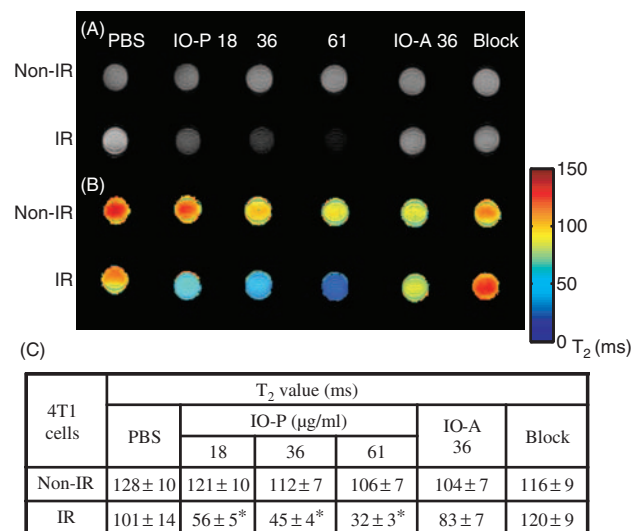
Figure 3. MRI measurements of reduction of T_2-weighted signal intensity (SI) and T_2 values due to specific binding of IO-PGN635F(ab′)$_2$ to exposed PS on cultured 4T1 cells. At 9.4T, MRI of homogeneous agar phantoms containing 3×10^5 4T1 cells that were pre-incubated with either PBS, different concentrations of IO-PGN635F(ab′)$_2$ (IO-P, [Fe] at 18, 36 and 61 μg/ml) or the control antibody conjugates, IO-AurexisF(ab′)$_2$ (IO-A at 36 μg/ml). (A) Minimal variations in SI were observed for the non-irradiated cells (top row). By contrast, the irradiated cells incubated with IO-PGN635F(ab′)$_2$ appeared darker (decreased SI) and maximal reduction of SI was observed at the highest iron concentration (61 μg/ml). Specific binding of IO-PGN635F(ab′)$_2$ to exposed PS was completely blocked by pre-treating the cells with unlabeled PGN635 antibodies. (B) Corresponding maps of T_2 relaxation time showed significant reduction of T_2 values for the irradiated cells incubated with IO-PGN635F(ab′)$_2$. Quantitative T_2 values were presented in (C) (*$p < 0.05$).

an increased number of hot-spots, typically seen as punctuate, were located in both central and peripheral regions of non-irradiated tumors (Fig. 6(A)), indicating baseline levels of PS exposure on tumor vascular endothelium. For the irradiated tumor, a dramatic increase in the number of hot-spots was observed after IO-PGN635F(ab′)$_2$. In addition to the punctate pattern, most hot-spots in the irradiated tumor are clustering (Fig. 6(A)). *In vivo* specific binding of IO-PGN635F(ab′)$_2$ was further confirmed by observing the lack of change in SI or hot-spots after injection of the control antibody conjugates, IO-AurexisF(ab′)$_2$. Dynamic change in fractions of hot-spots is plotted in Figure 6(C). For the group of tumors receiving IO-PGN635F(ab′)$_2$ ($n = 6$), mean fractions of hot-spots increased significantly in both the irradiated and non-irradiated tumors, with the maximal increase of $5.0 \pm 1.1\%$ and $2.7 \pm 0.4\%$, respectively ($p < 0.05$; Fig. 6(C)). Essentially no change was observed for the IO-AurexisF(ab′)$_2$ group ($n = 4$).

DISCUSSION
The present study demonstrates the feasibility of using PGN635F(ab′)$_2$-conjugated, PEGylated IO nanoparticles for *in vivo* MR imaging of PS exposed on vasculature of breast tumors. *In vivo* MRI detected inhomogeneous signal loss in peripheral and central regions of the tumors due to IO-PGN635F(ab′)$_2$ binding. In contrast to the punctate distribution pattern in non-irradiated tumors, clustering hypointense regions were seen after a single dose of 12 Gy radiation, indicating that IO-PGN635F(ab′)$_2$ can be used to detect increases in PS exposure induced by radiotherapy. The heterogeneous distribution of the nanoprobes detected by MRI correlated well with histological studies
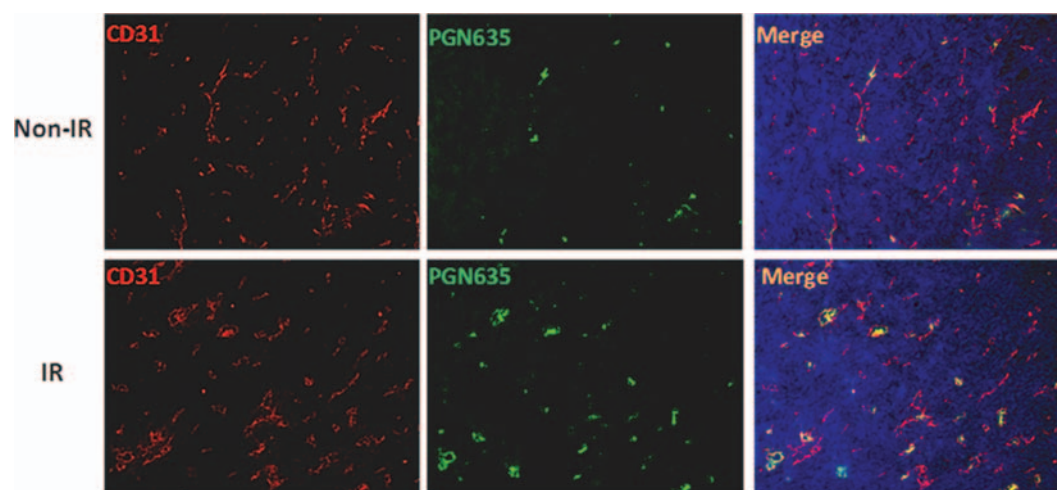
Figure 4. Immunohistochemical study of localization of PGN635 antibody in non-irradiated and irradiated tumors. Mice bearing a subcutaneous 4T1 tumor on each thigh received a single dose of 12 Gy irradiation to the left side tumor. Exposure of PS was determined 24 h later by i.v. injection of full length PGN635. Animals were perfused with saline 3 h later. Frozen sections of non-irradiated (top) and irradiated (bottom) tumors were analyzed for the presence of fluorescently labeled PGN635 (green). Vascular endothelial cells were counterstained with anti-CD31 (red). Nuclei were detected with DAPI (blue). Merged images revealed coincidence of staining showing that PGN635 was bound to vascular endothelial cells in the non-irradiated tumor. Increased PGN635 staining was seen in the irradiated tumors and was mainly due to increased staining of endothelial cells.

6
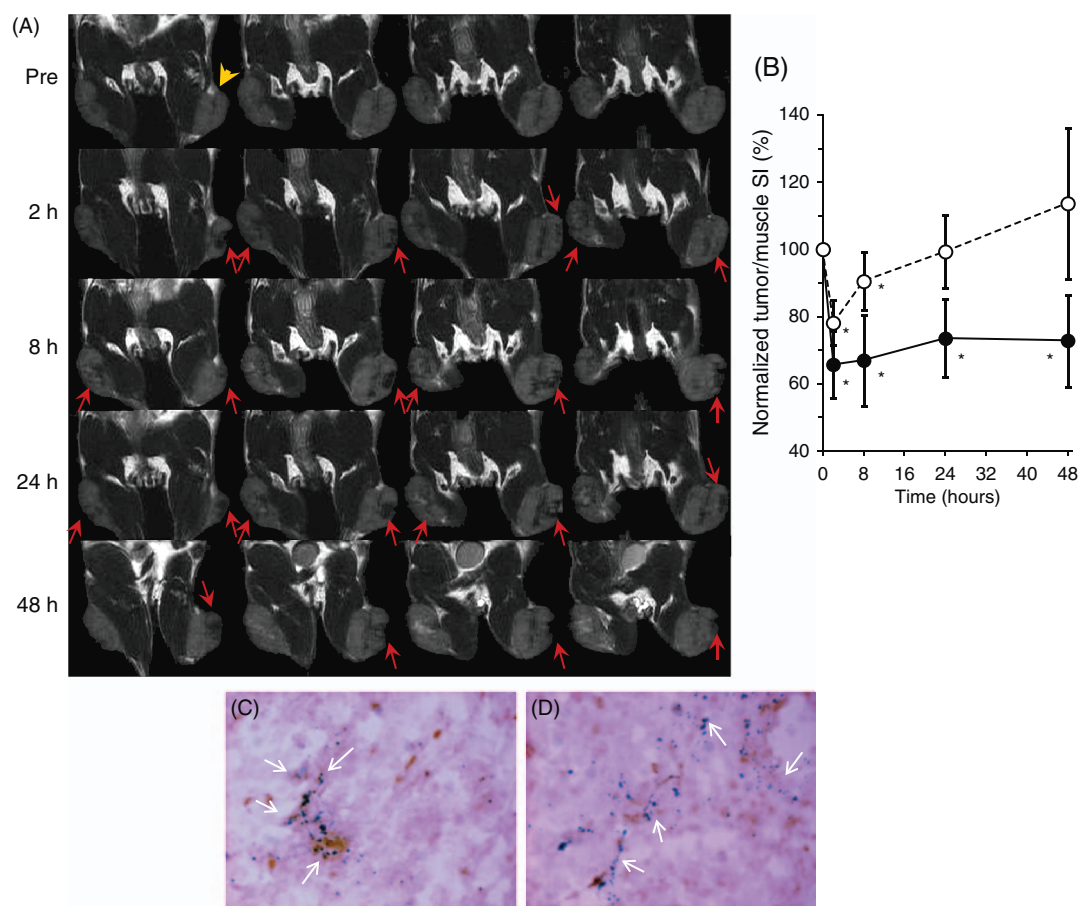
Figure 5. *In vivo* longitudinal study of exposed PS in 4T1 breast tumors by IO-PGN635F(ab')$_2$. (A) A representative mouse bearing size-matched subcutaneous 4T1 tumors on each thigh received 12 Gy of irradiation to the left tumor (arrowhead). Twenty-four hours after radiation, T_2-weighted fast spin echo multi-slice images (effective TE = 60 ms) were acquired at pre- and different time points post injection of IO-PGN635F(ab')$_2$ (2.5 mg Fe/kg) via tail vein. From 2 h post injection, marked regional signal drops (arrows) were clearly observed intratumorally on four consecutive coronal sections (thickness = 1 mm) of both side tumors, as compared to the pre-injection baseline images. The irradiated tumor had more hypointense regions than the non-irradiated tumor, indicating more PS exposure induced by radiation. (B) Plots of normalized T_2-weighted signal intensity (SI) change (tumor/thigh muscle) showed a maximal mean decrease of $22 \pm 7\%$ and $34 \pm 9\%$ for the non-irradiated (open circle) and irradiated (solid circle) tumor at 2 h, respectively. The signal decrease in the irradiated tumor persisted for at least 48 h after injection. However, SI of the non-irradiated tumor recovered gradually over time (*$p < 0.05$). (C) Double staining of iron (Prussian blue; blue) and vascular endothelial cells (anti-CD31; brown) revealed colocalization of iron with tumor vessels (arrows) in the non-irradiated tumor. (D) Increased iron staining (arrows) was seen in the irradiated tumors and was due to increased staining of endothelial cells.

showing that IO-PGN635F(ab')$_2$ localized specifically to tumor vascular endothelial cells. The antigen-binding specificity of IO-PGN635F(ab')$_2$ was verified by competition experiments with unconjugated PGN635 and by the lack of signal change with the non-binding control IO-AurexisF(ab')$_2$.

Much of the MRI data described in this report agree with our previous study using 800CW-PGN635F(ab')$_2$ for optical imaging of gliomas growing in mice.[18] A clear tumor contrast in non-irradiated U87 gliomas was visualized as early as 4 hrs after injection of 800CW-PGN635F(ab')$_2$ by near infrared optical imaging. Irradiation enhanced the tumor contrast in both subcutaneous and orthotopic U87 gliomas. However, the MRI data of the present study

differed from the optical data in both signal distribution and magnitude change. Optical signals appeared to be homogeneously derived from the whole tumor, while only small fractions of tumor regions were detected as hypointense by MRI (2.7% for non-irradiated and 5% for irradiated tumors; Figs. 5 and 6). Moreover, optical imaging revealed an tumor/normal ratio of ~ 3 for non-irradiated tumors and 4 for irradiated tumors, while 22% and 34% MRI signal intensity change was observed for the non-irradiated and irradiated tumor, respectively (Fig. 5(B)). These variations provide a good example of how the two imaging modalities differ in terms of sensitivity and spatial resolution. Compared to optical and nuclear imaging methods, MRI is limited by its inherent low sensitivity. Low concentration
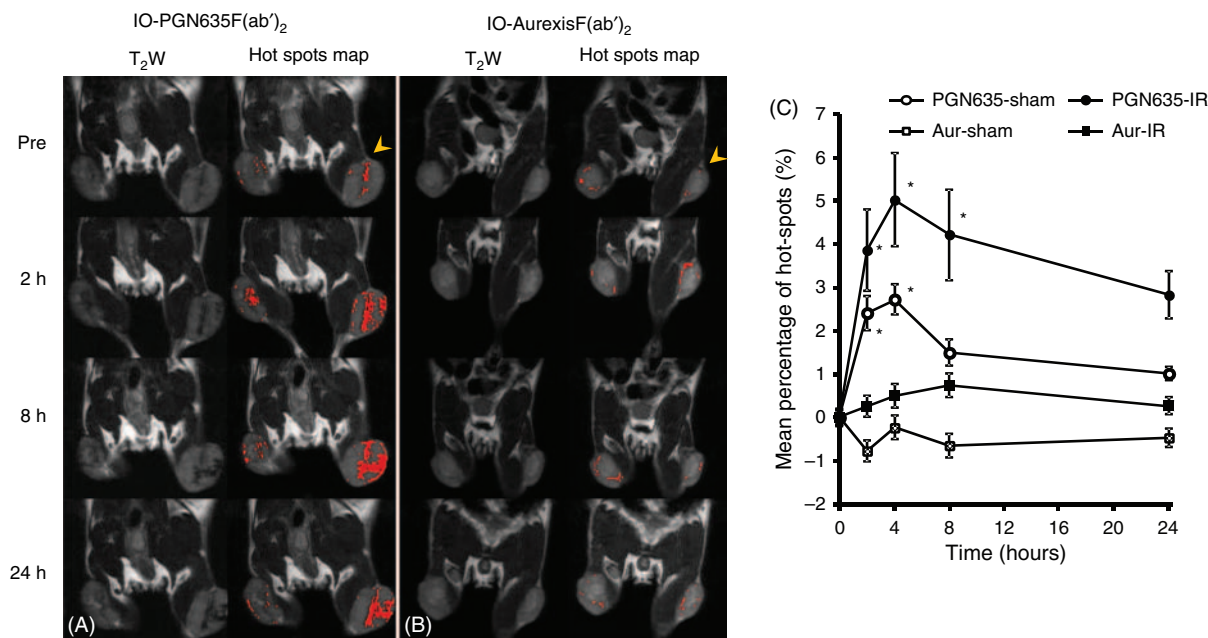
Figure 6. Quantitative 'hot spot' analysis of heterogeneous intratumoral distribution of IO-PGN635F(ab')$_2$. Hot-spots maps were created by identifying hypointense regions in tumor on T_2-weighted images and then overlapping them on the corresponding T_2-weighted images. (A) Baseline level of hot-spots prior to injection of IO-PGN635F(ab')$_2$ was presented in a representative non-irradiated and irradiated tumor (arrowhead; the same animal as shown in Fig. 4). Increased 'hot spots' were observed in both of the tumors after injection of IO-PGN635F(ab')$_2$. Compared to the non-irradiated tumor, the irradiated tumor appeared to have more 'hot spots.' (B) In contrast, there was essentially no change in 'hot spots' before and after injection of the control antibody conjugates, IO-AurexisF(ab')$_2$ in either a non-irradiated or irradiated tumor (arrowhead). (C) A fraction of 'hot spots' over the whole tumor was obtained for each of the tumors. Longitudinal changes in mean fractions of 'hot-spots' in the IO-PGN635F(ab')$_2$ ($n = 6$) or IO-AurexisF(ab')$_2$ group ($n = 4$) were plotted. After i.v. injection of IO-PGN635F(ab')$_2$, both the irradiated (solid circle) and non-irradiated (empty circle) tumors showed significant increase in the mean fraction of 'hot spots' (*$p < 0.05$). For the IO-AurexisF(ab')$_2$ group, no significant change was observed for either the irradiated (solid square) or non-irradiated (open square) tumors.

of contrast agents, e.g., in the nanomolar range, is insufficiently detectable by MRI, but can emit enough photons for optical imaging to capture. Thus, MRI imaging of IO-PGN635F(ab')$_2$ in this study may underestimate the tumor regions where PS is exposed on tumor vessels. However, the drawbacks of optical imaging such as light reflection, scattering and limited tissue penetration attribute to its low spatial resolution. We also noticed a difference in the intratumoral distribution between IO-PGN635F(ab')$_2$ and 800CW-PGN635F(ab')$_2$ in the irradiated tumors. In addition to tumor vascular localization, the optical 800CW-PGN635F(ab')$_2$ (dye:antibody = 1:1) were also seen binding to tumor cells after irradiation induced PS exposure. IO-PGN635F(ab')$_2$, which are IO nanoparticles conjugated with multiple large antibody fragments ($n = 18$), were exclusively confined to tumor vessels (Fig. 5(C)). This suggests that specific homing of the IO-PGN635F(ab')$_2$ to vasculature is responsible for the MRI signal change. Moreover, the data of the control antibody conjugates, IO-AurexisF(ab')$_2$ suggested a minimal enhanced permeability and retention (EPR) effect of the IO conjugates which has also been described in previous reports by others.[8, 21] Kiessling and colleagues have recently shown in their studies of $\alpha_v\beta_3$-targeted MR

imaging that RGD-conjugated SPIO (10 nm in diameter) are observed predominantly on $\alpha_v\beta_3$-expressing tumor vasculature of several mouse tumor models.[8] However, Xie et al. found that RGD-conjugated ultrasmall SPIO (4.5 nm) dramatically increased cellular uptake by tumor cells.[22] Thus, increasing particle size, e.g., by encapsulating IO into micelles or liposomes, will probably enhance vascular localization if blood vessels are the desired targets.[7]

Unlike the T_1 contrast agent, gadolinium-DTPA, SPIO is a T_2 contrast agent, which generates negative contrast on T_2 or T_2^*-weighted images. In comparison to paramagnetic T_1 contrast, SPIO has much higher molar relaxivity, thus, is widely used for molecular imaging applications by MRI.[23, 24] Signal loss due to SPIO shortening of T_2 relaxation time is often difficult to discriminate from background tissue with varying contrast, as induced by B_0 inhomogeneity or susceptibility artifacts. Moreover, regional signal increase during the longitudinal study was often observed in some of the tumors of the current study, which may be caused by pathophysiological changes such as edema, hemorrhage or necrotic formation. Given the small population of tumor vascular endothelial cells in tumor tissues, a simple analysis by comparing an average T_2 signal loss or T_2 reduction may compromise the interpretation

of signal change induced by targeted IO, proved to be less informative about spatial distribution of the vascular localized nanoprobes. Therefore, hot-spots analyses of the hypointense regions before and after injection of IO nanoprobes were applied to distinguish IO-induced signal voids from initial baseline level of dark signals, and gain spatial distribution information.

Successful cancer imaging requires imaging probes that recognize cancer-specific markers with great specificity and sensitivity.[25–27] Cell surface-exposed PS is an attractive target for molecular imaging. PS is strictly located in the inner leaflet of the plasma membrane bilayer in most normal cell types, including the vascular endothelium. Recent studies by Thorpe's lab have demonstrated that the oxidative stress within tumor microenvironment causes redistribution of phosphatidylserine (PS), the most abundant anionic phospholipid of the cell membrane, from the inner to the outer membrane leaflet of tumor endothelial cells.[10, 11] Vascular endothelium in normal tissues, even in those highly angiogenic ovarian blood vessels during ovulation, lacks exposed PS. Examination of a large panels of tumor types of mouse and rat models revealed that PS exposure on tumor vasculature is an universal phenomenon despite the extent of exposure varies between tumors.[13] Thus, development of PS targeted nanoparticle-based imaging contrast has a great potential for imaging various tumor types. The PS exposed endothelial cells are viable and not subjected to apoptotic process.[28, 29] These cells can resume growth and reestablish phospholipid asymmetry, which is distinct from the irreversible process occurring in cell death.[29, 30] Besides tumor vasculature, loss of PS asymmetry commonly occurs during apoptosis and necrosis.[30] Much interest has been generated in developing molecular imaging probes to noninvasively monitor the response of tumors to various treatments from the induction of tumor apoptosis.[27, 31] Annexin V is the PS binding ligand that is most widely used for this purpose. PGN635 and bavituximab, a chimeric monoclonal antibody that is currently evaluated in clinical trials,[32] have a more restricted specificity for PS than does annexin V, which recognizes PE in addition to PS and other anionic phospholipids.

CONCLUSIONS

In summary, we have developed a tumor vascular targeted imaging nanoprobe for MR imaging. By conjugating PGN635F(ab′)$_2$, a novel monoclonal PS targeting antibody, with PEG-coated iron oxide nanoparticles, we detect heterogeneous intratumoral distribution of the nanoprobes by MRI, which coincides with tumor vascular endothelial cells. Irradiation increases PS exposure of tumor vasculature, which leads to significantly increased MRI contrast. The high specificity of PGN635-IO nanoprobes establishes PS as an alternative and unique vascular biomarker for molecular imaging of tumor vasculatures.

REFERENCES

1. W. Cai and X. Chen, Multimodality molecular imaging of tumor angiogenesis. *J. Nucl. Med.* 49, 113S (**2008**).
2. A. P. Pathak, M. F. Penet, and Z. M. Bhujwalla, MR molecular imaging of tumor vasculature and vascular targets. *Adv. Genet.* 69, 1 (**2010**).
3. D. A. Sipkins, D. A. Cheresh, M. R. Kazemi, L. M. Nevin, M. D. Bednarski, and K. C. Li, Detection of tumor angiogenesis *in vivo* by alphaVbeta3-targeted magnetic resonance imaging. *Nat. Med.* 4, 623 (**1998**).
4. M. Jin, G. Hao, X. Sun, and W. Chen, Nanoparticle-based positron emission tomography and single photon emission computed tomography imaging of cancer. *Rev. Nanosci. Nanotechnol.* 1, 3 (**2012**).
5. W. Cai, G. Niu, and X. Chen, Imaging of integrins as biomarkers for tumor angiogenesis. *Curr. Pharm. Des.* 14, 2943 (**2008**).
6. P. M. Winter, S. D. Caruthers, A. Kassner, T. D. Harris, L. K. Chinen, J. S. Allen, E. K. Lacy, H. Zhang, J. D. Robertson, S. A. Wickline, and G. M. Lanza, Molecular imaging of angiogenesis in nascent Vx-2 rabbit tumors using a novel alpha(nu)beta3-targeted nanoparticle and 1.5 tesla magnetic resonance imaging. *Cancer Res.* 63, 5838 (**2003**).
7. C. Khemtong, C. W. Kessinger, J. Ren, E. A. Bey, S. G. Yang, J. S. Guthi, D. A. Boothman, A. D. Sherry, and J. Gao, *In vivo* off-resonance saturation magnetic resonance imaging of alphavbeta3-targeted superparamagnetic nanoparticles. *Cancer Res.* 69, 1651 (**2009**).
8. F. Kiessling, J. Huppert, C. Zhang, J. Jayapaul, S. Zwick, E. C. Woenne, M. M. Mueller, H. Zentgraf, M. Eisenhut, Y. Addadi, M. Neeman, and W. Semmler, RGD-labeled USPIO inhibits adhesion and endocytotic activity of alpha v beta3-integrin-expressing glioma cells and only accumulates in the vascular tumor compartment. *Radiology* 253, 462 (**2009**).
9. O. Schnell, B. Krebs, J. Carlsen, I. Miederer, C. Goetz, R. H. Goldbrunner, H. J. Wester, R. Haubner, G. Popperl, M. Holtmannspotter, H. A. Kretzschmar, H. Kessler, J. C. Tonn, M. Schwaiger, and A. J. Beer, Imaging of integrin alpha(v)beta(3) expression in patients with malignant glioma by [18F] Galacto-RGD positron emission tomography. *Neuro Oncol* 11, 861 (**2009**).
10. S. Ran, A. Downes, and P. E. Thorpe, Increased exposure of anionic phospholipids on the surface of tumor blood vessels. *Cancer Res.* 62, 6132 (**2002**).
11. S. Ran and P. E. Thorpe, Phosphatidylserine is a marker of tumor vasculature and a potential target for cancer imaging and therapy. *Int. J. Radiat Oncol. Biol. Phys.* 54, 1479 (**2002**).
12. X. Huang, M. Bennett, and P. E. Thorpe, A monoclonal antibody that binds anionic phospholipids on tumor blood vessels enhances the antitumor effect of docetaxel on human breast tumors in mice. *Cancer Res.* 65, 4408 (**2005**).

13. P. E. Thorpe, Vascular targeting agents as cancer therapeutics. *Clin. Cancer Res.* 10, 415 (**2004**).

14. S. Ran, J. He, X. Huang, M. Soares, D. Scothorn, and P. E. Thorpe, Antitumor effects of a monoclonal antibody that binds anionic phospholipids on the surface of tumor blood vessels in mice. *Clin. Cancer Res.* 11, 1551 (**2005**).

15. T. A. Luster, J. He, X. Huang, S. N. Maiti, A. J. Schroit, P. G. de Groot, and P. E. Thorpe, Plasma protein beta-2-glycoprotein 1 mediates interaction between the anti-tumor monoclonal antibody 3G4 and anionic phospholipids on endothelial cells. *J. Biol. Chem.* 281, 29863 (**2006**).

16. M. Jennewein, M. A. Lewis, D. Zhao, E. Tsyganov, N. Slavine, J. He, L. Watkins, V. D. Kodibagkar, S. O'Kelly, P. Kulkarni, P. P. Antich, A. Hermanne, F. Rosch, R. P. Mason, and P. E. Thorpe, Vascular imaging of solid tumors in rats with a radioactive arsenic-labeled antibody that binds exposed phosphatidylserine. *Clin. Cancer Res.* 14, 1377 (**2008**).

17. D. E. Gerber, A. T. Stopeck, L. Wong, L. S. Rosen, P. E. Thorpe, J. S. Shan, and N. K. Ibrahim, Phase I safety and pharmacokinetic study of bavituximab, a chimeric phosphatidylserine-targeting monoclonal antibody, in patients with advanced solid tumors. *Clin. Cancer Res.* 17, 6888 (**2011**).

18. D. Zhao, J. H. Stafford, H. Zhou, and P. E. Thorpe, Near-infrared optical imaging of exposed phosphatidylserine in a mouse glioma model. *Transl. Oncol.* 4, 355 (**2011**).

19. H. Zhou, K. Luby-Phelps, B. E. Mickey, A. A. Habib, R. P. Mason, and D. Zhao, Dynamic near-infrared optical imaging of 2-deoxyglucose uptake by intracranial glioma of athymic mice. *PLoS One* 4, e8051 (**2009**).

20. H. Zhou, M. Chen, and D. Zhao, Longitudinal MRI evaluation of intracranial development and vascular characteristics of breast cancer brain metastases in a mouse model. *PLoS One* 8, e62238 (**2013**).

21. C. W. Kessinger, C. Khemtong, O. Togao, H. Takahashi, B. D. Sumer, and J. Gao, *In vivo* angiogenesis imaging of solid tumors

22. by alpha(v)beta(**3**)-targeted, dual-modality micellar nanoprobes. *Exp. Biol. Med.* (*Maywood*) 235, 957 (**2010**).

22. J. Xie, K. Chen, H. Y. Lee, C. Xu, A. R. Hsu, S. Peng, X. Chen, and S. Sun, Ultrasmall c(RGDyK)-coated Fe_3O_4 nanoparticles and their specific targeting to integrin alpha(v)beta3-rich tumor cells. *J. Am. Chem. Soc.* 130, 7542 (**2008**).

23. J. W. Bulte and D. L. Kraitchman, Iron oxide MR contrast agents for molecular and cellular imaging. *NMR Biomed.* 17, 484 (**2004**).

24. D. L. Thorek, A. K. Chen, J. Czupryna, and A. Tsourkas, Superparamagnetic iron oxide nanoparticle probes for molecular imaging. *Ann. Biomed. Eng.* 34, 23 (**2006**).

25. R. Weissleder and M. J. Pittet, Imaging in the era of molecular oncology. *Nature* 452, 580 (**2008**).

26. L. Yang, X. H. Peng, Y. A. Wang, X. Wang, Z. Cao, C. Ni, P. Karna, X. Zhang, W. C. Wood, X. Gao, S. Nie, and H. Mao, Receptor-targeted nanoparticles for *in vivo* imaging of breast cancer. *Clin. Cancer Res.* 15, 4722 (**2009**).

27. M. Zhao, D. A. Beauregard, L. Loizou, B. Davletov, and K. M. Brindle, Non-invasive detection of apoptosis using magnetic resonance imaging and a targeted contrast agent. *Nat. Med.* 7, 1241 (**2001**).

28. A. K. Hammill, J. W. Uhr, and R. H. Scheuermann, Annexin V staining due to loss of membrane asymmetry can be reversible and precede commitment to apoptotic death. *Exp. Cell Res.* 251, 16 (**1999**).

29. B. Mirnikjoo, K. Balasubramanian, and A. J. Schroit, Mobilization of lysosomal calcium regulates the externalization of phosphatidylserine during apoptosis. *J. Biol. Chem.* 284, 6918 (**2009**).

30. K. Balasubramanian and A. J. Schroit, Aminophospholipid asymmetry: A matter of life and death. *Annu. Rev. Physiol.* 65, 701 (**2003**).

31. T. Nakajima, K. Sano, M. Mitsunaga, P. L. Choyke, and H. Kobayashi, Real-time monitoring of *in vivo* acute necrotic cancer cell death induced by near infrared photoimmunotherapy using fluorescence lifetime imaging. *Cancer Res.* 72, 4622 (**2012**).

32. A. Tomillero and M. A. Moral, Gateways to clinical trials. *Methods Find Exp. Clin. Pharmacol.* 31, 661 (**2009**).